branching and cyclization occurs. Here, we refer to the pregel stage of vinyl–divinyl copolymerization as an example.[21] If we choose a cyclopolymerization process as one extreme and random cyclization of linear or branched chains as the other, the vinyl–divinyl polymerization could be placed somewhere between these two extremes.[22] A short distance between a reaction center and a reactive site in the process favors[23] formation of separated cycles along a linear primary chain. On the other hand, conformational behavior of most commonly used divinyl cross-linking agents and the presence of previously formed large cycles randomize cycle sizes. Obviously, the reaction sites, i.e., side chains with unreacted vinyls, may remain unchanged as well.

For the randomly cyclized linear chains, very simple reasoning[24] leads to the relation first given by Allen et al.[25]

$$g_\infty(\min) = 1/(r + 1) \tag{47}$$

where r is the number of cross-links (contacts[24]) existing in the cyclized volumeless chain. Equation 45 provides a similar relation for the other extreme, while eq 36 describes, as a kind of reference, a case when long side chains belonging to a cross-linking agent are not involved in any cyclization but provide extensive branching instead. The relations above offer a new method for calculating the configurational behavior of idealized Gaussian molecules. Furthermore, the method has wider applicability and in particular suggests some general trends for dimensions of vinyl–divinyl primary molecules.[21]

Acknowledgment. Professor J. W. Kennedy is greatly acknowledged for reading the manuscript and valuable comments. The work was supported by the Committee of Chemical Sciences of the Polish Academy of Sciences.

References and Notes

(1) Flory, P. J. "Principles of Polymer Chemistry"; Cornell University Press: Ithaca, NY, 1953.
(2) For references, see, e.g.: Ross-Murphy, S. B. In "Macromolecular Chemistry"; Jenkins, A. D.; Kennedy, J. F., Editors; Royal Society: London, 1980.
(3) Zimm, B. H.; Stockmayer, W. H. *J. Chem. Phys.* **1949**, *17*, 1301.
(4) Dobson, G. R.; Gordon, M. *J. Chem. Phys.* **1964**, *41*, 2389. Gordon, M.; Malcolm, G. N.; Butler, D. S. *Proc. R. Soc. London, Ser. A* **1966**, *295*, 29.
(5) Fixman, M. *J. Chem. Phys.* **1962**, *36*, 306.
(6) Forsman, W. C. *Macromolecules* **1968**, *1*, 343.
(7) Šolc, K. *Macromolecules* **1973**, *6*, 378.
(8) Eichinger, B. E. *J. Polym. Sci., Polym. Symp.* **1976**, *No. 54*, 127.
(9) Eichinger, B. E. *Macromolecules* **1980**, *13*, 1.
(10) Eichinger, B. E. *Macromolecules* **1972**, *5*, 496.
(11) Eichinger, B. E. *Macromolecules* **1977**, *10*, 671.
(12) Martin, J. E.; Eichinger, B. E. *J. Chem. Phys.* **1978**, *69*, 4588. Eichinger, B. E.; Martin, J. E. *Ibid.* **1978**, *69*, 4595.
(13) Gupta, S. K.; Forsman, W. C. *Macromolecules* **1973**, *6*, 285. Gupta, S. K.; Forsman, W. C. *Ibid.* **1974**, *7*, 853. Gupta, S. K.; Forsman, W. C. *Ibid.* **1972**, *5*, 779.
(14) Šolc, K. *Macromolecules* **1972**, *5*, 705.
(15) Essam, J. W.; Fisher, M. E. *Rev. Mod. Phys.* **1970**, *42*, 272.
(16) Kirchhoff matrices describe graphs uniquely although not conversely. The matrix **A** (**B**) describes a graph having all units and links of the structural element, but vertex degrees of two (one) terminal units are increased by one.
(17) Bryant, P. R. In "Graph Theory and Theoretical Physics"; Harary, F., Editor; Academic Press: New York, 1967.
(18) Matrices essentially identical with the Kirchhoff matrices of linear chain graphs often arise in solving problems involving certain differential equations. They were first applied for studying polymers by Rouse (Rouse, P. E. *J. Chem. Phys.* **1953**, *21*, 1272), and his matrix was identical, in terms of symbols used here, with the matrix **A**. The matrix used by Zimm (Zimm, B. H. *J. Chem. Phys.* **1956**, *24*, 269) was exactly the Kirchhoff matrix of a linear chain. By deleting the first row and the first column in the Zimm matrix, one can obtain the matrix here called **B**.
(19) Flory, P. J. "Statistical Mechanics of Chain Molecules"; Interscience: New York, 1969.
(20) Berry, G. C.; Orofino, T. A. *J. Chem. Phys.* **1964**, *40*, 1614.
(21) Dušek, K.; Galina, H.; Mikeš, J. *Polym. Bull.* **1980**, *3*, 19.
(22) Dušek, K.; Prins, W. *Adv. Polym. Sci.* **1969**, *6*, 1.
(23) *Jackobson*, H.; Stockmayer,W. H. *J. Chem. Phys.* **1950**, *18*, 1600.
(24) Gordon, M.; Torkington, J. A.; Ross-Murphy, S. B. *Macromolecules* **1977**, *10*, 1090. Torkington, J. A. Thesis, Essex University, 1979.
(25) Allen, G.; Burgess, J.; Edwards, S. F.; Walsh, D. J. *Proc. R. Soc. London, Ser. A* **1973**, *334*, 453, 465, 477.

New Method for Estimating the Parameters of the Wormlike Chain Model from the Intrinsic Viscosity of Stiff-Chain Polymers

Miloslav Bohdanecký

Institute of Macromolecular Chemistry, Czechoslovak Academy of Sciences, 162 06 Prague 6, Czechoslovakia. *Received November 9, 1982*

ABSTRACT: It has been found that the term Φ_0 in the Yamakawa–Fujii equation for the intrinsic viscosity of the wormlike continuous cylinder model, $[\eta]_0 = \Phi_0(\lambda^{-1})^{3/2}L^{1/2}/M_L$, can be given a simple form valid over a broad range of the chain contour length L: $\Phi_0 = \Phi_{0,\infty}[B_0 + A_0(\lambda^{-1}/L)^{1/2}]^{-3}$. The parameter A_0 is a function of the ratio d/λ^{-1} while B_0 is nearly constant. On the basis of these results, new methods are proposed for evaluating the model parameters (Kuhn segment length λ^{-1}, relative molecular mass per unit contour length M_L, and chain diameter d) from the intrinsic viscosity data for stiff-chain polymers. Accordingly, the plot of $(M^2/[\eta])^{1/3}$ vs. $M^{1/2}$ is linear, and the random-coil value of $\langle R_0^2\rangle/M$, i.e., $(\langle R_0^2\rangle/M)_\infty$, is simply evaluated from the slope of the plot. The possibilities of estimating M_L and d, either from the intrinsic viscosity data alone or, preferably, from their combination with the partial specific volume of the polymer, are discussed. The procedures are applied to nine typical stiff-chain polymers (polyisocyanate, cellulose trinitrate, polypeptides in helical conformation, aromatic polyamides, etc.). The results agree well with those obtained by more involved procedures. The effect of the excluded volume on the shape of the plot is also qualitatively discussed.

Introduction

The category of stiff-chain polymers includes important natural and synthetic macromolecular substances, the number of which steadily increases. Since the determination of molecular dimensions by means of the light-scattering method is frequently difficult with these substances, their conformational characteristics are derived from the hydrodynamic quantities, mainly from the in-

0024-9297/83/2216-1483$01.50/0

trinsic viscosity. The procedures advanced for this purpose are based on theories[1-5] representing linear polymer chains by the wormlike chain model, particularly on the theory of Yamakawa and Fujii.[6]

The latter is an application of the Oseen–Burgers procedure of hydrodynamics to the wormlike continuous cylinder model, i.e., a cylinder, the axis of which is described by a space curve obeying the wormlike chain statistics. It is characterized by the contour length L, the effective hydrodynamic diameter d, and the persistence length $^1/_2\lambda^{-1}$ (or the Kuhn statistical segment length λ^{-1}). One limit of the model ($L \to 0$, $d \to 0$) is the rigid straight cylinder (or rod), and the other ($L \to \infty$) is the random-flight chain. For the latter case we can write

$$(\langle R_0^2\rangle/L)_\infty \equiv \lim_{L\to\infty} (\langle R_0^2\rangle/L) = \lambda^{-1} \tag{1a}$$

$$\lambda^{-1} = (\langle R_0^2\rangle/M)_\infty M_L \tag{1b}$$

or

$$\lambda^{-1} = 6(\langle S_0^2\rangle/M)_\infty M_L \tag{1c}$$

Here, M is the relative molecular mass, $\langle R_0^2\rangle$ is the mean-square end-to-end distance of the chain, and $\langle S_0^2\rangle$ is the mean-square radius of gyration of the chain (both unperturbed by the excluded-volume effect). M_L is the shift factor defined as the relative molecular mass per unit contour length; $M_L = M/L$.

Evaluation of the parameters $(\langle R_0^2/M\rangle_\infty$, λ^{-1}, M_L, and d from the intrinsic viscosity data suffers from serious and restrictive difficulties. Some procedures (e.g., plotting $M/[\eta]$ vs. $M^{1/2}$ or $M^{1/2}/[\eta]$ vs. $M^{-1/2}$ and extrapolating to $M^{1/2} \to 0$ or to $M^{-1/2} \to 0$, respectively)[7,8] may be used only with systems where the exponent, ν', of the Mark–Houwink–Kuhn–Sakurada (MHKS) equation is considerably lower than about 0.9.[9] Another method, involving nonlinear extrapolation to $M \to 0$ of the plot of $[\eta]/M^2$ vs. M, has been proposed for systems with higher ν' values.[10,11] A more general method involves finding the theoretical best-fit curve to logarithmic plots of $[\eta]/M^{1/2}$ vs. $M^{1/2}$ or of $M^2/[\eta]$ vs. M.[6,12] The fitting of curves is not free from ambiguity, even if the viscosity data are combined with the results of other methods (e.g., sedimentation coefficient[13,14]).

In this paper we present a new method for treating the intrinsic viscosity data for stiff-chain polymers. We show that the function $F_1(L,d)$ of the Yamakawa–Fujii theory of the intrinsic viscosity[6] can be expressed, with good accuracy and over a broad range of chain lengths, in a simple analytic form which, on rearrangement, provides a basis for the estimation of $(\langle R_0^2\rangle/M)_\infty$, the fundamental conformational characteristic. We also discuss the possibilities of estimating M_L and d. By means of the outlined methods, we analyze the dependences of the intrinsic viscosity on the relative molecular mass for several typical stiff-chain polymers. Most of them have been chosen so that the values of $(\langle R_0^2\rangle/M)_\infty$ obtained from viscosity can be checked against the results of the light-scattering method.

Theory

Fundamental Relationships. The analysis of the intrinsic viscosity of stiff-chain polymers can conveniently be started with eq 43 in ref 6

$$[\eta]_0 = \Phi_0 L_r^{3/2}(\lambda^{-1})^3/M \tag{2}$$

where $[\eta]_0$ (expressed in $cm^3\ g^{-1}$) is the intrinsic viscosity corresponding to a configuration of the chain unperturbed by the excluded-volume effect and Φ_0 is the viscosity function depending on L_r and d_r, where L_r is the reduced contour length and d_r is the reduced diameter

$$L_r = L/\lambda^{-1} \tag{3a}$$

$$d_r = d/\lambda^{-1} \tag{3b}$$

The limit of Φ_0 for $L_r \to \infty$, denoted by $\Phi_{0,\infty}$, is independent of d_r and equal to 2.86×10^{23}.[6] By combining eq 1–3, we obtain

$$[\eta]_0 = [\Phi_{0,\infty}(\langle R_0^2\rangle/M)_\infty^{3/2} M^{1/2}]F_1 \tag{4}$$

where

$$F_1 = \Phi_0/\Phi_{0,\infty} \tag{5}$$

The term in square brackets on the right-hand side of eq 4 is identical with the Flory–Fox formula for the intrinsic viscosity of unperturbed random coils in the nondraining limit (cf. ref 15). The factor F_1 is a function of L_r and d_r. At $L_r \to \infty$, it is equal to unity for all values of d_r. The values of F_1 for $10^{-3} \le d_r \le 1$ and $0.1 \lesssim L_r \lesssim 10^4$ are given in ref 6.

It follows from eq 4 that for stiff-chain polymers the values of $[\eta]_0/M^{1/2}$ converge to $K_{0,\infty} = \Phi_{0,\infty}(\langle R_0^2\rangle/M)_\infty^{3/2}$ at high values of L_r. Thus, estimation of $(\langle R_0^2\rangle/M)_\infty$ depends on the possibility of extrapolating F_1 to $L_r \to \infty$. As the formulas for F_1 given in ref 6 are too complicated, they do not allow a simple extrapolation. We believe that the approximate analytic expression for $F_1(L_r)$ to be presented and discussed in the following can facilitate this operation.

Approximate Expression for $F_1(L_r)$. In Figure 1 we have plotted $L_r^{1/2}/F_1^{1/3}$ vs. $L_r^{1/2}$. Except for the lowest values of $L_r < L_r^*$, the dependences for all values of d_r appear to be linear, indicating that the equation

$$L_r^{1/2}/F_1^{1/3} = A_0 + B_0 L_r^{1/2} \tag{6}$$

could be a fair approximation to F_1. A careful analysis, however, reveals a slight curvature of the plot. That can be demonstrated in the following way. If the parameters A_0 and B_0 are evaluated by the least-squares method from a complete set of available F_1 values (for $0.5 \le L_r \le 10^4$) and if they are substituted into eq 6 to yield F_1, the differences between the original and calculated F_1 values are small (about 1 or 2%) at $L_r > 10$ but significant (about 5% or more) at $L_r < 10$.

If, however, the range of L_r values covered by the present approximation is reduced to $L_r^* \le L_r \le L_r^{**}$ (where L_r^* and L_r^{**} are given in Table I) and if the new values of A_0

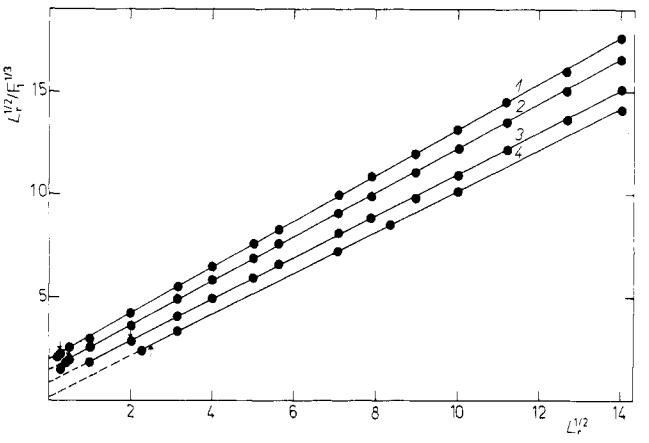

Figure 1. Plot of theoretical data according to eq 6. (●) Theoretical values from ref 6 for $d_r = 10^{-3}$, 10^{-2}, 10^{-1}, and 4×10^{-1} (curves 1–4). Full straight lines are best-fit ones calculated according to eq 6 with A_0 and B_0 given in Table I. L_r^* denoted by arrows.

Table I
Parameters of Eq 7

			range of validity					range of validity	
d_r	A_0	B_0	L_r*	L_r**	d_r	A_0	B_0	L_r*	L_r**
10^{-3}	2.004	1.113	0.1	200	8×10^{-2}	1.022	1.010	3.2	2×10^3
2×10^{-3}	1.909	1.089	0.2	300	10^{-1}	0.966	1.000	4.0	2×10^3
5×10^{-3}	1.704	1.079	0.4	300	1.4×10^{-1}	0.722	1.012	10	2×10^4
10^{-2}	1.542	1.066	0.4	300	2×10^{-1}	0.550	1.005	16	2×10^4
2×10^{-2}	1.376	1.052	1.0	400	4×10^{-1}	0.0317	0.9986	5	10^6
5×10^{-2}	1.120	1.031	1.0	500	6×10^{-1}	−0.583	0.999	10^2	10^6
6×10^{-2}	1.070	1.025	2.0	10^3	1.0	−1.426	0.999	2×10^2	10^6
7×10^{-2}	1.053	1.016	2.0	10^3					

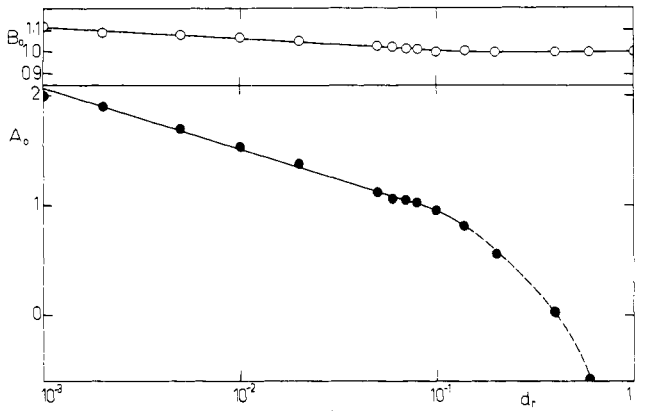

Figure 2. Dependence on d_r of the parameters A_0 (●) and B_0 (○). Values from Table I. Full lines calculated according to eq 8 and 9, respectively.

and B_0 (Table I) are used to calculate F_1, the correspondence between the original and calculated values is significantly improved. Hence, the formula

$$F_1 = (B_0 + A_0/L_r^{1/2})^{-3} \tag{7}$$

easily obtained from eq 6, offers a good approximation to F_1 over an interval of more than 2 orders of magnitude in L_r.[16]

Both parameters of eq 7 depend on the reduced diameter d_r (Figure 2). The dependences can be described by eq 8 and 9:

$$B_0 = 1.00 - 0.0367 \log d_r \tag{8}$$

$$A_0 = 0.46 - 0.53 \log d_r \tag{9}$$

The former is valid for $d_r \leq 1$ with an accuracy of about 1.5%, and the latter for $d_r \leq 0.1$ with an accuracy of about 3%. B_0 is a slowly decreasing function of d_r, and in the first approximation it may be replaced by the mean value, $\bar{B}_0 = 1.05$. The dependence of A_0 on d_r is more pronounced. At $d_r \gtrsim 0.1$, A_0 steeply decreases so that for $d_r \gtrsim 0.4$, it becomes negative (Figure 2).

New Method of Plotting the [η] Data. Combining eq 4, 7, and 1 leads to the equation

$$[\eta]_0 = [\Phi_{0,\infty}(\langle R_0^2\rangle/M)_\infty^{3/2}M^{1/2}] \times [B_0 + A_0(\langle R_0^2\rangle/M)_\infty^{1/2}M_L/M^{1/2}]^{-3} \tag{10}$$

which can be rearranged into a form suitable for application

$$(M^2/[\eta]_0)^{1/3} = A_\eta + B_\eta M^{1/2} \tag{11}$$

where

$$A_\eta = A_0 M_L \Phi_{0,\infty}^{-1/3} \tag{12}$$

and

$$B_\eta = B_0 \Phi_{0,\infty}^{-1/3}(\langle R_0^2\rangle/M)_\infty^{-1/2} \tag{13}$$

According to these equations, $(\langle R_0^2\rangle/M)_\infty$ can simply be evaluated from the slope B_η of the plot of $(M^2/[\eta])^{1/3}$ vs. $M^{1/2}$. The intercept A_η depends on d_r (through A_0) and on M_L so that, for an estimation of either of them, one needs additional information. In the following part we discuss the possibility of obtaining this information from the coordinates of the minimum on the plot of $M/[\eta]_0$ vs. $M^{1/2}$ or from the partial specific volume of the polymer.

Analysis of the Plots of $M/[\eta]_0$ vs. $M^{1/2}$ and Estimation of d_r and M_L. It has been shown[9] that the plots of $L_r^{1/2}/F_1$ vs. $L_r^{1/2}$ (at constant $d_r \lesssim 0.1$) display a minimum, the coordinates of which, $(L_r^{1/2}/F_1)_m$ and $L_{r,m}^{1/2}$, depend on d_r. They are simply related to the parameters A_0 and B_0. To demonstrate that, we rearrange eq 6 into the form

$$L_r^{1/2}/F_1 = (A_0 + B_0 L_r^{1/2})^3/L_r \tag{14}$$

differentiate with respect to $L_r^{1/2}$, and apply the condition of the minimum. We find that

$$L_{r,m}^{1/2} = 2A_0/B_0 \tag{15}$$

and

$$(L_r^{1/2}/F_1)_m = (27/4)A_0 B_0^2 \tag{16}$$

The values of $L_{r,m}^{1/2}$ and $(L_r^{1/2}/F_1)_m$ for a few typical values of d_r are presented in Table III. Since eq 6 is an approximation, it is worthwhile to check these results against the accurate ones.

It follows from eq 1–5 that

$$M/[\eta]_0 = [\Phi_{0,\infty}^{-1}(\langle R_0^2\rangle/M)_\infty^{-1}M_L]L_r^{1/2}/F_1 \tag{17}$$

and

$$L_{r,m}^{1/2} = M^{1/2}(\langle R_0^2\rangle/M)_\infty^{-1/2}M_L^{-1} \tag{18}$$

For $L_r > 2.278$, the function F_1 may be expressed in the form

$$F_1 = 1 - \sum_{i=1}^{4} C_i L_r^{-i/2} \tag{19}$$

where the numerical coefficients C_i are complicated functions of d_r (cf. ref 6). By substituting from eq 19 into (17), differentiating with respect to $L_r^{1/2}$, and introducing the condition of the minimum, we have

$$1 + \sum_{i=2}^{4}(i-1)C_i L_{r,m}^{-i/2} = 0 \tag{20}$$

The values of $L_{r,m}$ are obtained by numerically solving eq 20, and the values of $(L_r^{1/2}/F_1)_m$ are calculated from $L_{r,m}$ by means of eq 4 and 19. An inspection of the entries in Table II shows that eq 15 and 16 allow an approximate estimation of $L_{r,m}$ and a fairly good estimation of $(L_r^{1/2}/F_1)_m$.

According to Figure 3, the dependences of $(L_r^{1/2}/F_1)/(L_r^{1/2}/F_1)_m$ on $(L_r/L_{r,m})^{1/2}$ for different values of d_r overlap

Table II
Comparison between Original and Approximate Values of F_1^{-1}

	d_r							
	10^{-3}		10^{-2}		5×10^{-2}		10^{-1}	
L_r	*a*	*b*	*a*	*b*	*a*	*b*	*a*	*b*
0.1	410	413.7	145.1	209.9				
0.25	139.3	134	64.2	71.5				
0.32	104.2	99.1	*51.2*	54.5				
0.5	62.3	61.5	33.8	34.2	*15.04*	17.88		
1	29.5	30.3	17.7	17.7	9.19	9.94	6.27	7.59
2	15.4	16.2	9.95	10.03	6.01	6.05	*4.28*	4.77
4	9.16	9.46	6.14	6.20	4.00	4.02	3.10	3.25
5	7.89	8.11	5.36	5.41	3.57	3.59	2.83	2.94
8	5.96	6.04	4.16	4.19	2.89	2.90	2.36	2.41
10	5.30	5.32	3.74	3.75	2.66	2.65	2.19	2.22
16	4.25	4.20	3.08	3.06	2.27	2.25	1.90	1.91
100	2.29	2.27	1.83	1.82	1.51	1.49	1.33	1.31
200	*1.92*$_5$	1.97$_5$	1.60	1.62	1.36	1.36	1.23	1.21$_5$
320	1.74	1.84	*1.48*	1.53	1.29	1.31	1.16	1.17
500	1.60	1.74	1.39	1.46	*1.23*	1.26	1.13	1.13$_5$
1000	1.425	1.63	1.28	1.38	1.17	1.21	*1.11*	1.09

[a] Original values.[6] [b] Values calculated by means of eq 7 with A_0 and B_0 given in Table I. Range of validity of eq 7 denoted by italics.

Table III
Coordinates of the Minimum of the Plot of $L_r^{1/2}/F_1$ vs. $L_r^{1/2}$

	$L_{r,m}^{1/2}$ calcd		$(L_r^{1/2}/F_1)_m$ calcd	
d_r	eq 20	as $2A_0/B_0$	eq 4 and 19	as $(27/4)A_0B_0^2$
10^{-3}	3.277	3.601	16.22	17.01
2×10^{-3}	3.103	3.504	14.96	15.33
5×10^{-3}	2.927	3.158	13.33	13.31
10^{-2}	2.774	2.894	11.79	11.78
2×10^{-2}	2.594	2.616	10.12	10.18
5×10^{-2}	2.152	2.173	7.96	7.95
6×10^{-2}	1.992	2.088	7.49	7.44
7×10^{-2}	1.830	2.073	7.14	7.01

almost perfectly at $(L_r/L_{r,m})^{1/2} > 1$ but are distinct at $(L_r/L_{r,m})^{1/2} < 1$. This fact can, in principle, be used for a rough estimation of the diameter d_r.

Equations 17 and 19 indicate that the dependence of $L_r^{1/2}/F_1$ on $L_r^{1/2}$ is a generalized form of the plot of $M/[\eta]_0$ vs. $M^{1/2}$ (ref 9) and that the coordinates of the minimum of the former, $(L_r^{1/2}/F_1)_m$ and $L_{r,m}^{1/2}$, stand in a simple relationship to those of the latter, $(M/[\eta]_0)_m$ and $M_m^{1/2}$.

Now, if the values of $(M/[\eta]_0)_m$ and $M_m^{1/2}$ have been estimated, we can plot, on the same scale, the experimental data as $(M/[\eta]_0)/(M/[\eta]_0)_m$ vs. $(M/M_m)^{1/2}$ and the theoretical data (for several values of d_r) as $(L_r^{1/2}/F_1)/(L_r^{1/2}/F_1)_m$ vs. $(L_r/L_{r,m})^{1/2}$, and look for the theoretical curve that matches the experimental dependence. In this way the reduced d_r is assessed. We then estimate A_0 by interpolating in Figure 2 or by employing eq 9 and calculate M_L from A_η according to eq 12.

The plots of $M/[\eta]_0$ vs. $M^{1/2}$ are sensitive to errors in $[\eta]_0$ and M so that direct estimation of $(M/[\eta]_0)_m$ and $M_m^{1/2}$ may be inaccurate. There exist, however, simple relationships, similar to eq 15 and 16, between these coordinates and the parameters A_η and B_η, viz.

$$(M/[\eta]_0)_m = (27/4)A_\eta B_\eta^2 \quad (21)$$

and

$$M_m^{1/2} = 2A_\eta/B_\eta \quad (22)$$

which facilitate the estimation of $(M/[\eta]_0)_m$ and $M_m^{1/2}$.

It will be shown later that, with the usual accuracy of experimental data, the procedure just described hardly yields the diameter d_r with an accuracy better than ±40%.

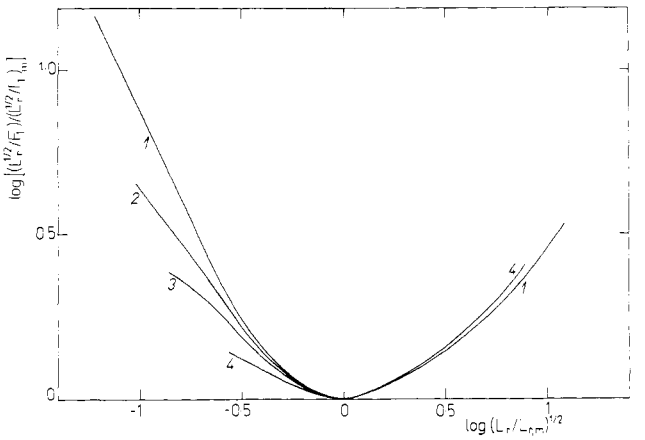

Figure 3. Generalized plot of $M/[\eta]$ vs. $M^{1/2}$. Curves 1–4 calculated for $d_r = 10^{-3}$, 10^{-2}, 2×10^{-2}, and 5×10^{-2}, respectively. $(L_r^{1/2}/F_1)_m$ and $L_{r,m}^{1/2}$ values characterize the minimum point on the plots of $L_r^{1/2}/F_1$ vs. $L_r^{1/2}$. For details, see text.

The estimation is particularly difficult (or impossible) with data covering a narrow span of M values. Nevertheless, as demonstrated by Figure 2, a difference of 100% in d_r (at $d_r \leq 0.1$) corresponds to a difference of only 10% in A_0. Thus, even if d_r is not determined exactly, the shift factor M_L can still be estimated with fair accuracy.

Alternative Way of Estimating d_r. Tsuji et al.[14] made the assumption that the hydrodynamic volume occupied by 1 g of the wormlike cylinder is equal to the partial specific volume, $\bar{v}$, of the polymer molecules, so that

$$\bar{v} = (\pi N_A/4)(d^2/M_L) \quad (23)$$

By combining eq 23 with (1b), (3b), (12), and (13) and by substituting $B_0 \equiv \bar{B}_0 = 1.05$, we obtain

$$d_r^2/A_0 = (4\Phi_{0,\infty}/1.215\pi N_A)(\bar{v}/A_\eta)B_\eta^4 \quad (24)$$

Thus, having determined $(\bar{v}/A_\eta)B_\eta^4$, we can evaluate the reduced diameter d_r via the dependence of d_r^2/A_0 on d_r (Figure 4), which can be described by the approximate empirical formulas

$$\log (d_r^2/A_0) = 0.173 + 2.158 \log d_r \quad (d_r \leq 0.1) \quad (25a)$$

$$\log (d_r^2/A_0) = 0.795 + 2.78 \log d_r \quad (0.1 \leq d_r \leq 0.4) \quad (25b)$$

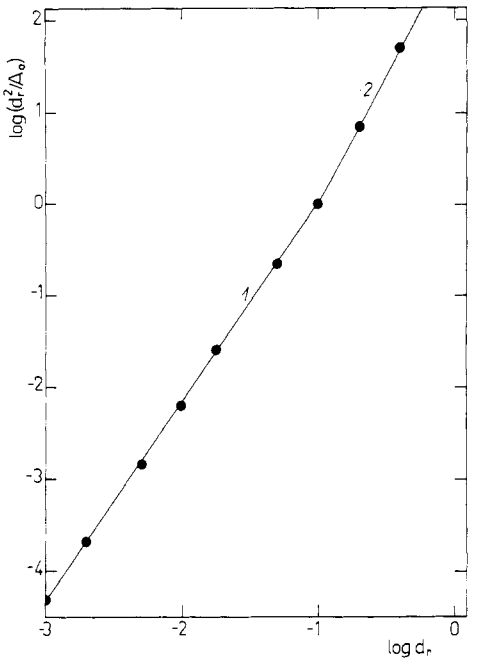

Figure 4. Logarithmic dependence of d_r^2/A_0 on d_r. (●) Values of d_r^2/A_0 calculated from data in Table I. Lines 1 and 2 calculated according to eq 25a and 25b, respectively.

The assumption underlying eq 23 seems reasonable for chains which are stiff so that their local shape may be regarded as cylindrical.[17] It may be objected that, in general, the diameter in eq 23 need not be identical with the effective hydrodynamic diameter d. Our primary aim, however, is to estimate M_L from A_η. To do that, we need to know A_0, which, fortunately, is not a very sensitive function of d_r (at least for $d_r \leq 0.1$) and, consequently, is not much affected by inaccuracy of d_r. In comparison with the procedure described in the preceding paragraph, this method is more accurate and is to be preferred whenever possible.

Excluded-Volume Effect. In the theory underlying the present methods, the excluded-volume effect and the expansion of molecular dimensions are neglected. This assumption need not be met in practice. It is therefore useful to consider the impact that the expansion could have on the plot of $(M^2/[\eta])^{1/3}$ vs. $M^{1/2}$.

Let us start with the equation

$$\alpha_\eta^3 = [\eta]/[\eta]_0 = 1 + C_\eta z + \ldots \quad (26)$$

where α_η^3 is the viscosity expansion factor, $[\eta]$ is the intrinsic viscosity for expanded molecules, and z is the well-known excluded-volume parameter (proportional to $L_r^{1/2}$ or $M^{1/2}$[15]). Stockmayer and Yamakawa[18] found theoretically that, in the equation for the mean-square end-to-end distance

$$\alpha_R^2 = \langle R^2\rangle/\langle R_0^2\rangle = 1 + C_R z + \ldots \quad (27)$$

the coefficient C_R is a function of L_r. It is zero at $L_r \leq 1$, equal to 0.671 at $L_r = 10$, and close to the limiting (random coil) value, $^{134}/_{105}$, at $L_r \gtrsim 10^3$. The dependence of C_η on L_r is unknown at present. Assuming that it will be similar to that of C_R, we can expect that the viscosity expansion factor will not be negligible at very high values of L_r but will be very close to unity at low L_r (of the order of unity) so that the initial slope of the plot of $(M^2/[\eta])^{1/3}$ vs. $M^{1/2}$ will not be significantly affected by expansion.

The situation is less favorable with an alternative plot[16,17] based on a simple transformation of eq 11, namely, $(M^{1/2}/[\eta])^{1/3}$ vs. $M^{-1/2}$. It involves extrapolation to $M^{-1/2} \to 0$. Regarding the excluded-volume effect (particularly with less stiff chains at high chain length), which would affect this extrapolation in an unpredictable way, we consider this alternative less suitable.

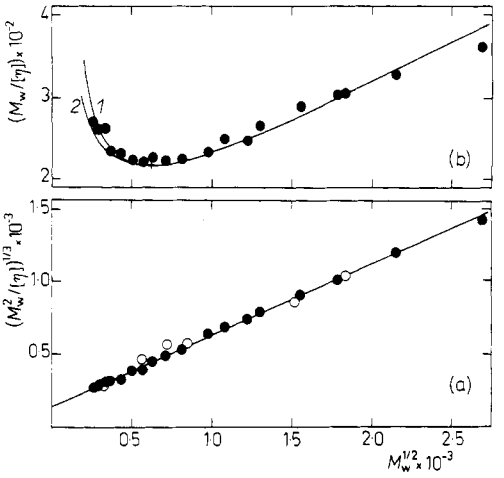

Figure 5. Poly(*n*-hexyl isocyanate): (a) Plot of $(M^2/[\eta])^{1/3}$ vs. $M^{1/2}$; (b) plot of $M/[\eta]$ vs. $M^{1/2}$. Data for hexane solutions (25 °C): (●) ref 23; (○) ref 21. Curves 1 and 2 in (b) calculated for $d_r \times 10^2 = 2$ and 5, respectively. The minimum point in (b) calculated by means of eq 21 and 22 is denoted by a cross.

Discussion

In the following the proposed methods will be employed to analyze the intrinsic viscosity data for a few typical stiff-chain polymers chosen so that their Mark–Houwink–Kuhn–Sakurada exponents ν' cover the range from 0.7 to 1.7.

Poly(*n*-hexyl isocyanate). Poly(*n*-hexyl isocyanate) (PHIC) exhibits nonlinear logarithmic dependences of $[\eta]$ on M[20–23] and a minimum in the plot of $M/[\eta]$ vs. $M^{1/2}$ (Figure 5). The data of Murakami et al.,[23] covering a span of relative molecular masses from 0.068×10^6 to 7.2×10^6, are particularly suited for checking the methods outlined above. The treatment based on eq 11 gives for $(\langle S_0^2\rangle/M)$ a value that is in excellent agreement with that obtained by the light-scattering method (Table IV).

The position of the minimum on the plot of $M/[\eta]$ vs. $M^{1/2}$ is well established by calculation according to eq 22, but the shape of the plot does not allow an accurate estimation of d_r. Nevertheless, regarding the small scatter of the data points, we try to estimate a probable value of d_r. The superposition of experimental and calculated dependences is better for $d_r = 0.02$ than for $d_r = 0.05$ (Figure 5b). Using the corresponding A_0, we obtain $M_L = 710$ nm^{-1}, $\lambda^{-1} = 84$ nm, and $d = 1.7$ nm. A less ambiguous result is obtained by means of the method based on eq 24: $M_L = 680$ nm^{-1}, $\lambda^{-1} = 82$ nm, and $d = 1.3$ nm. The values agree well with those reported by Murakami et al.[23] (Table IV).

By using the entries in Table III (for $d_r = 0.02$), we identify $M_m^{1/2} = 0.62 \times 10^3$ with $L_r^{1/2} \simeq 2.6$ and find that the highest relative molecular mass, 7.24×10^6, corresponds to $L_r = 134$ and is within the range of validity of eq 11 (cf. Table I).

The plots of $(M^2/[\eta])^{1/3}$ vs. $M^{1/2}$ for PHIC in other solvents are also linear and their slopes depend on the solvent used. Since the plots of $M/[\eta]$ vs. $M^{1/2}$ do not allow d_r to be estimated and no data are available for the partial specific volume in these solvents, only the values of $(\langle R_0^2\rangle/M)_\infty$ have been determined. They show (Table IV) that the PHIC chains are more extended in nonpolar solvents.

Extracellular Polysaccharide Schizophyllan in Helical Conformation. There are no light-scattering data

Table IV
Model Parameters of Some Stiff-Chain Polymers[a]

solvent	$(\langle R_0^2\rangle/M)_\infty \times 10^2$, nm²	M_L, nm⁻¹	λ^{-1}, nm	d, nm	viscosity data from ref
		Poly(n-hexyl isocyanate)			
hexane	12 (12[b])	680 (715)	82 (84)	1.3 (1.6)	21, 23
toluene	10.7				
THF	8.2				20, 22
CCl_4	13.1				
$CHCl_3$	7.4				
CCl_4/TFAA	6.4				
		Schizophyllan			
water	14	1900 (2200)	274 (400)	1.6 (2.6)	25
		Pt Complex (PPBD)			
benzene	3.8	680 (810)	25 (26)	0.35 (1.2)	26
		Cellulose Trinitrate			
acetone	5.8	500 (524[c])	29 (33[c])	1.0	31
	5.7 (6.1[b,d])	610	36	1.1	32
	5.4 (5.0[b,e])	900	49	1.3	32
ethyl acetate	8.0	590	46	0.89	33
	6.8	600	41	0.98	34
		Poly(ε-carbobenzoxy-L-lysine) (PCBL)			
DMF	5.2	1450	76	0.58	28
		1500–1680	79–88	0.8–1.75	
		Poly(γ-ethyl L-glutamate) (PELG)			
DMF	9.1	980–1040	84–94	0.8–1.9	29

[a] Values of d and M_L are estimated by means of eq 24, and those for PCBL in the second row and for PELG from the plots of $M[\eta]$ vs. $M^{1/2}$ (see text). Values in parentheses are taken from original papers (unless stated otherwise). Abbreviations: TFAA, trifluoroacetic acid; THF, tetrahydrofuran; DMF, dimethylformamide; PPBD, *catena*-μ-1,4-butadiynediyl-*trans*-bis(tributylphosphine)platinum. [b] Recalculated as $6(S_0^2/M)$ from the light-scattering data given in the original papers. [c] Reference 6. [d] 13.9% N. [e] 12.9% N.

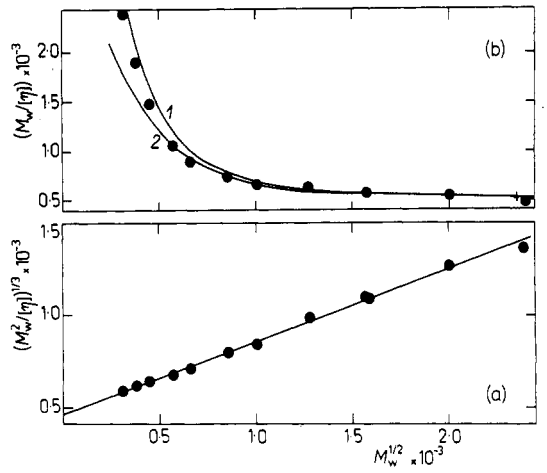

Figure 6. Schizophyllan: (a) Plot of $(M^2/[\eta])^{1/3}$ vs. $M^{1/2}$; (b) plot of $M/[\eta]$ vs. $M^{1/2}$. Data for solutions in water (25 °C), ref 25. Curves 1 and 2 in (b) calculated for $d_r = 10^{-3}$ and 10^{-2}, respectively. The probable minimum is denoted by cross.

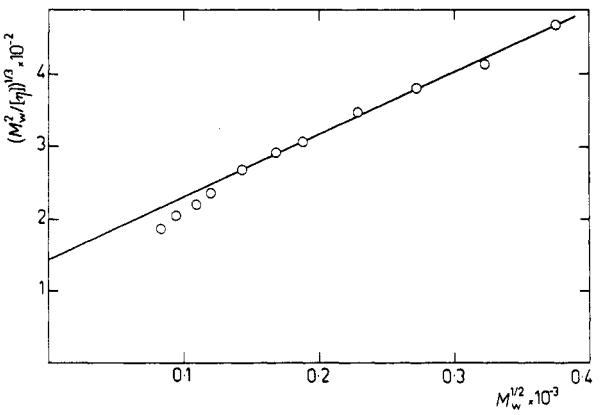

Figure 7. *catena*-μ-1,4-Butadiynediyl-*trans*-bis(tributylphosphine)platinum in benzene at 25 °C.[26]

available for the dimensions of schizophyllan molecules in water, and information about its stiffness resides in a combination of the viscosity and sedimentation data.[25] By analyzing the intrinsic viscosity data by means of the methods proposed in this paper, we decline somewhat from the intention of checking them against the results of the light-scattering method. However, the MHKS exponent for schizophyllan in water being 1.7 at $M \lesssim 0.5 \times 10^6$ and 1.2 at $M > 5 \times 10^6$, the polymer is very suitable for checking the proposed methods.

The plots of $(M^2/[\eta])^{1/3}$ vs. $M^{1/2}$ and $M/[\eta]$ vs. $M^{1/2}$ are presented in Figure 6. The ratio $(\langle R_0^2\rangle/M)_\infty = 1.4 \times 10^{-2}$ nm² evaluated from the former is very high (Table IV). Calculated curves 1 and 2 in Figure 6b correspond to $d_r = 10^{-3}$ and 10^{-2}, respectively. Using the latter, we obtain $M_L = 2050$ nm⁻¹, $\lambda^{-1} = 296$ nm, and $d = 3.0$ nm. These values agree rather well with those found by Yanaki et al.[25] By employing the method based on eq 24 with $\bar{v} = 0.691$,[25] we find lower values: $M_L = 1900$ nm⁻¹, $\lambda^{-1} = 274$ nm, and $d = 1.6$ nm (Table IV).

The lowest relative molecular mass, $M_w = 9.6 \times 10^4$, corresponds to $L_r = 0.185$. Since for $6 \le d_r \times 10^3 \le 10$, our approximation to the function F_1 is valid at $L_r \gtrsim 0.4$; the first three points in Figure 6 are to be left out from consideration when fitting the dependence to a straight line.

***catena*-μ-1,4-Butadiynediyl-*trans*-bis(tributylphosphine)platinum (PPBD).** When plotted according to eq 11, the data points for PPBD[26] display downward deviations at $M^{1/2} \le 120$ (Figure 7). Neglecting these points, we obtain $(\langle R_0^2\rangle/M)_\infty = 3.6 \times 10^{-2}$ nm². The plot of $M/[\eta]$ vs. $M^{1/2}$ exhibits a minimum but the shape is such

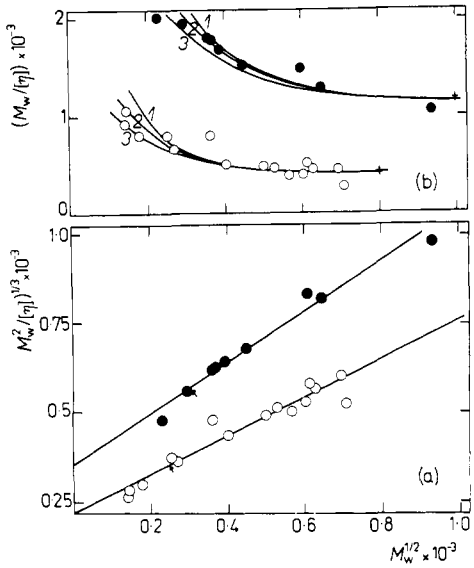

Figure 8. Polypeptides: (a) Plot of $(M^2/[\eta])^{1/3}$ vs. $M^{1/2}$; (b) plot of $M/[\eta]$ vs. $M^{1/2}$. Data points: (○) Poly(γ-ethyl L-glutamate);[29] (●) poly(ε-carbobenzoxy-L-lysine)[28] in dimethylformamide (25 °C). Curves 1–3 in (b) calculated for $d_r = 10^{-3}$, 10^{-2}, and 2×10^{-2}, respectively. Arrows in (a) indicate approximate lower bounds to the validity of eq 7 for $d_r = 10^{-2}$.

that an estimation of d_r is impossible. By means of eq 24 with $\bar{v} = 0.776$,[26] we obtain values of M_L and λ^{-1} that agree very well with those reported by Motowoka et al.[26] (Table IV). The difference in d is remarkable.

The relative molecular mass per Kuhn statistical segment is about 22×10^3, which means that the segment contains about 40 monomer units. The reduced contour length L_r of the lowest fraction is only 0.31. That may explain deviations from linearity in Figure 7 at low values of M.

Polypeptides. The molecules of polypeptides and poly(α-amino acids) in perfectly helical conformation are assumed to have a rodlike shape. Thus the MHKS exponent should lie close to 1.8, and according to Daune, Freund, and Spach,[27] the plot of $M^2/[\eta]$ vs. log M should be linear. In reality, the exponents are lower, and the DFS plots are nonlinear with most polymers of this group. This indicates that the molecules are not rodlike and that perturbations of the helical structure make the chain less rigid. Thus the wormlike chain appears to be a more suitable model for both the equilibrium and hydrodynamic properties, and checking this idea by means of the intrinsic viscosity data may be an interesting task.

Unfortunately, very few papers contain both the intrinsic viscosity and the radius of gyration for fractions of good quality over a broad range of relative molecular mass. The studies of poly[ε-carbobenzoxy-L-lysine] (PCBL) by Matsuoka et al.[28] and of poly[γ-ethyl L-glutamate] (PELG) by Terbojevich et al.[29] are exceptions to this rule. Their data are plotted as $(M^2/[\eta])^{1/3}$ vs. $M^{1/2}$ and as $M/[\eta]$ vs. $M^{1/2}$ in Figure 8.

Theoretical curves in Figure 8b for three values of d_r have been drawn so as to have their minimum point at M_m calculated according to eq 22 from the values of A_η and B_η. It is seen that the experimental values of $M/[\eta]$ are not accurate enough to allow an unambiguous estimation of d_r. Consequently, only spans of M_L, λ^{-1}, and d can be given (Table IV). The lower values correspond to $d_r = 10^{-2}$, and the higher ones to $d_r = 2 \times 10^{-2}$. The span is narrow for M_L and λ^{-1} but, as can be expected, it is broad for d. Lower values of all parameters resulted from calculations for PCBL by means of eq 24 with $\bar{v} = 0.803$ cm³/g.[28]

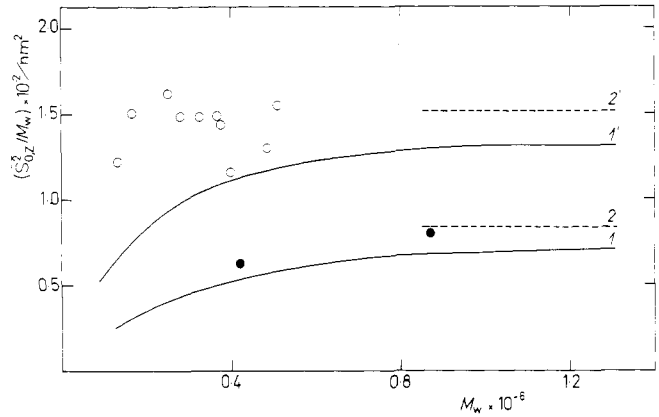

Figure 9. Molar mass dependence of $\langle S_0^2 \rangle_z / M_w$ for polypeptides. Notation of data points as in Figure 8. Full curves 1 and 1′ calculated according to eq 28 with the values of $(\langle R_0^2 \rangle / M)_\infty$ and M_L given in Table IV. Broken horizontal lines 2 and 2′ correspond to $(\langle S_0^2 \rangle / M)_\infty$.

Figure 9 represents the dependence of $\langle S_0^2 \rangle / M$ on M calculated according to the Benoît–Doty equation[30]

$$\langle S_0^2 \rangle / M = (\langle S_0^2 \rangle / M)_\infty \{1 - (3a/L) \times [1 - 2(a/L) + 2(a/L)^2 - 2(a/L)^2 \exp(-L/a)]\} \quad (28)$$

where $L = M/M_L$. It is remarkable that at $M > 1 \times 10^6$, both polypeptides should assume the configuration close to the random coil, despite the presence of helical sections in the chain. The curves are compared with the light-scattering radii of gyration. Data points for two PCBL fractions measured by Matsuoka et al.[28] lie only slightly above the curve, and their dependence on the relative molecular mass has the expected trend.

With PELG, the situation is less easy to understand. Experimental values of $\langle S_0^2 \rangle / M$[29] are almost independent of M, which is at variance with expectation. The differences between the experimental and calculated values of $\langle S_0^2 \rangle / M$ at low relative molecular masses are very large and can hardly be ascribed to the effect of polydispersity. They are lower (10–35%) at $M > 1 \times 10^5$ and could perhaps be accounted for by polydispersity.

The Kuhn segment length is about 76 nm for PCBL and 90 nm for PELG, and the number of monomer units per segment is ~430 for the former and ~500 for the latter polymer.

By means of the values of M_L and λ^{-1} in Table IV, we can assess the range of relative molecular masses for which the approximation to $F_1(L_r)$ by eq 7 may be used. The lowest bounds to validity of eq 7 are denoted by arrows in Figure 8. It is seen that the lowest two or three data points should be omitted from the extrapolation.

Cellulose Trinitrate. The intrinsic viscosity data for cellulose trinitrate in acetone[31,32] and ethyl acetate[33,34] are plotted as $(M^2/[\eta])^{1/3}$ vs. $M^{1/2}$ in Figure 10. The plots are linear at $M \lesssim 1 \times 10^6$; the slight downward curvature at higher relative molecular masses might stem from the nonadequacy of eq 11 at higher values of L_r and/or from the excluded-volume effect. The highest relative molecular mass ($M \simeq 4 \times 10^6$) corresponds to $L_r \simeq 300$ and is within the interval of validity of eq 11. Curvature of the plots can, therefore, be ascribed to the expansion due to the excluded-volume effect.

The values of $(\langle S_0^2 \rangle / M)$ calculated from the initial slopes B_η agree very well with the values of $\langle S_0^2 \rangle_z / M_w$ for the highest relative molecular mass obtained from the light-scattering radii of gyration (after correction for the coil expansion) (Table IV).

The plots of $M/[\eta]$ vs. $M^{1/2}$ display minima but the scatter of the data points precludes using them for an

Table V
Model Parameters of Isomeric Poly(phthaloyl-*trans*-2,5-dimethylpiperazines)

solvent	$(\langle R_0^2\rangle/M)_\infty \times 10^2$, nm^2	M_L, nm^{-1}	λ^{-1}, nm	d, nm	viscosity data from ref
		Poly(*o*-phthaloyl-*trans*-2,5-dimethylpiperazine)[b]			
NMP[c]	1.6 (2.1)[a]	390 (330; 370*)	6.2 (6.6; 5.9*)	0.71 (0.74; 0.66*)	17
$CHCl_3$	1.9	380 (330)	7.2 (7.4)	0.78 (0.73)	17
m-cresol	2.0_5	340 (350)	6.9 (9.2)	0.74 (0.75)	17
HFIP	1.9_5	320 (330)	6.2 (8.2)	0.70 (0.71)	17
DMA	1.4_5	380 (310)	5.6 (5.6)	0.70 (0.72)	17
HAc	1.6	400 (320)	6.3 (6.6)	0.80 (0.71)	17
		Poly(terephthaloyl-*trans*-2,5-dimethylpiperazine)[b]			
TFE	2.9_5 (3.7^a)	370 (350; 370*)	11 (12.8; 11*)	0.78 (0.76; 0.81*)	35
m-cresol	3.6	290 (310)	10.5 (14.8)	0.69 (0.71)	35
		Poly(isophthaloyl-*trans*-2,5-dimethylpiperazine)[b]			
TFE	2.4	440	10.5 (6.2)	0.86	36
m-cresol	2.8	340	9.6 (9.8)	0.75	36

[a] Evaluated from $\langle S_0^2\rangle/M$ given in ref 17 and 36. [b] Values of M_L, λ^{-1}, and d in parentheses are taken from the original papers;[17,35,36] those denoted by asterisks are from ref 37. [c] Abbreviations: NMP, *N*-methylpyrrolidone; HFIP, hexafluoro-2-propanol; DMA, dimethylacetamide; HAc, acetic acid; TFE, trifluoroethanol.

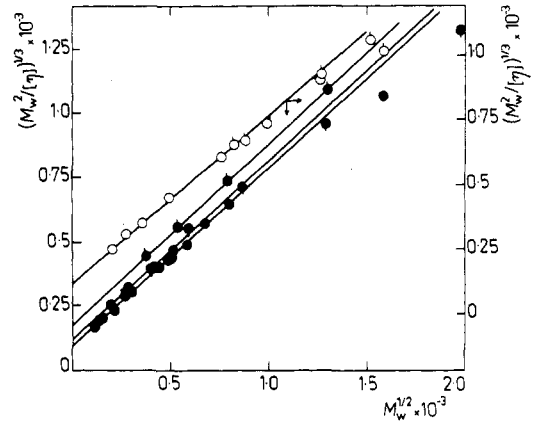

Figure 10. Cellulose trinitrate. Solutions in acetone (left-hand scale): (●) ref 31; (◐) 13.9% N; (◉) 12.9% N, ref 32. Solutions in ethyl acetate (right-hand scale): (○) ref 33; (◇) ref 34.

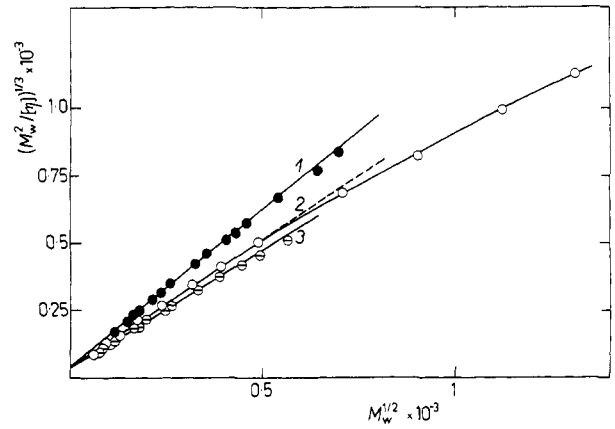

Figure 11. Isomeric poly(phthaloyl-*trans*-2,5-dimethylpiperazines). Solutions in *m*-cresol (25 °C): curve 1, PPDP;[17] curve 2, PIDP;[35] curve 3, PTDP.[36]

estimation of d_r. The values of d_r and M_L have, therefore, been estimated from the intercepts A_η and the partial specific volumes (from ref 31 and 33) by means of eq 24. The values of M_L (Table IV) compare well with the value $M_L = 570$ nm^{-1} calculated from the relative molecular mass M_0 and the length of the repeat unit l ($M_0 = 297$, $l = 0.517$ nm). Crystallographic diameter oscillates between 0.27 and 0.86 nm (cf. ref 6). By combining Meyerhoff's viscosity and sedimentation data, Yamakawa and Fujii[6] found d = 0.4 nm.

Polyamides PPDP, PIDP, and PTDP. The hydrodynamic behavior of poly(*o*-phthaloyl-*trans*-2,5-dimethylpiperazine) (PPDP), poly(terephthaloyl-*trans*-2,5-dimethylpiperazine) (PTDP), and poly(isophthaloyl-*trans*-2,5-dimethylpiperazine) (PIDP) exhibits some interesting features.[17,35,36] The plots of log $[\eta]$ vs. log M are nonlinear and their slopes (ν') decrease as the relative molecular mass increases; e.g., for PIDP, ν' is close to 0.94 at low M and about 0.75 at $M > 6 \times 10^4$. The latter value is in the range usually observed for long flexible polymer chains in good solvents, but the former is an indication of stiffness. There is also a good deal of independent evidence for the excluded-volume effect, at least for PIDP at $M > 1 \times 10^5$.[36]

The combined effects of stiffness and the excluded volume complicate the analysis of the intrinsic viscosity data. For this reason, we include the three isomeric polyamides in the present discussion, pursuing the following aims: (i) We wish to check the use of the method based on eq 11 for less stiff chains than those discussed so far. (ii) By analyzing the data for PIDP, we hope to find out if the method allows the effects of chain stiffness and expansion to be separated. (iii) Motowoka et al.[17,35] have found that the theory of Yamakawa and Fujii cannot account for the experimental data for PPDP and PTDP at $M < 2 \times 10^4$. We wish to explore the possibility of detecting such deviations by the proposed method.

As demonstrated by Figure 11, the plots of $(M^2/[\eta])^{1/3}$ vs. $M^{1/2}$ (for solutions in *m*-cresol) are linear at $0.15 \le M^{1/2} \times 10^{-3} \le 0.5$ but exhibit downward deviations above the latter value. The deviations are very mild with PPDP and PTDP and very strong with PIDP (where the range of $M^{1/2}$ values is substantially broader). The plots for other solvents are similar. The deviations are assigned to the excluded-volume effect.

With respect to these facts, the $(\langle R_0^2\rangle/M)_\infty$ values must be calculated from the initial slopes, and the accuracy of the results is poorer than for the previous systems. It is remarkable that the values of $(\langle R_0^2\rangle/M)_\infty$ calculated with $\Phi_{0,\infty} = 2.86 \times 10^{23}$ (Table V) are lower by about 20–30% than those evaluated from the radii of gyration.[17,35,36] The agreement would be improved by using a lower value of $\Phi_{0,\infty}$ ($(2.1\text{–}2.2) \times 10^{23}$). Despite this discrepancy, the values of $(\langle R_0^2\rangle/M)_\infty$ give evidence of pronounced solvent effects on the chain conformation and confirm the effect of the structure of the phthalic acid isomers (cf. ref 36).

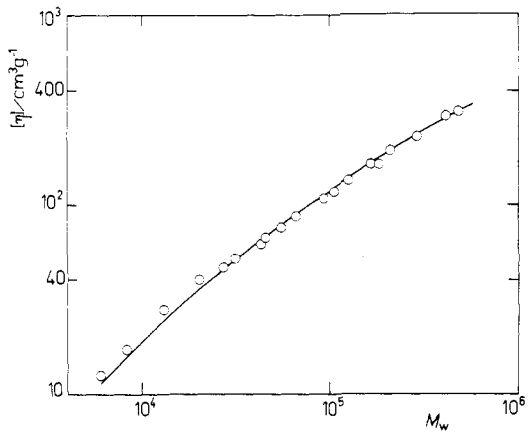

Figure 12. Plot of $[\eta]$ vs. M_w for poly(*o*-phthaloyl-*trans*-2,5-dimethylpiperazine) in *N*-methylpyrrolidone. Data points from ref 17. Curve calculated by means of eq 10.

The values of M_L and d estimated by means of eq 24 for PTDP are in good correspondence with those reported by Motowoka et al.[35] and with those estimated, in a different way, by Yamakawa and Yoshizaki.[37] For PPDP, the agreement with the results in ref 37 is very good but is less good with those in ref 17. As follows from eq 24, the value of M_L calculated from A_η depends to some extent on the value of $\Phi_{0,\infty}$. Using $\Phi_{0,\infty} \times 10^{-23} = 2.1$ instead of 2.86 would reduce M_L by about 12%. Nevertheless, comparison of the M_L values for PPDP in NMP (Table V, first row) obtained by different methods from the same set of experimental data illustrates difficulties inherent in the estimation of M_L in this case.

The plots in Figure 11 for *m*-cresol (and for some other solvents as well) display slight downward deviations at $M \lesssim 15 \times 10^3$. In Figure 12 we compare the logarithmic plot of $[\eta]$ vs. M for PPDP with the curve calculated according to eq 10. The curve fits the data quite well at $M > 15 \times 10^3$ but does not fit so well below this value. Since the reduced contour lengths for all fractions lie within the range of validity of eq 7 for $d_r \leq 0.1$ (cf. Figure 1), the deviations in Figures 11 and 12 have to be assigned to some effects that the theory does not take into account. As shown by Figure 11, such effects can be detected by plotting data according to eq 11.

Concluding Remarks

It has been shown that the plot of the intrinsic viscosity data according to eq 11 simplifies the estimation of $(\langle R_0^2\rangle/M)_\infty$ or $(\langle S_0^2\rangle/M)_\infty$ for stiff-chain polymers. Combining the parameter A_η of eq 11 with other data, preferably with the partial specific volume of the polymer, leads to reasonably accurate values of the shift factor M_L and the effective hydrodynamic diameter d.

The starting point of the methods proposed here is the theory of the intrinsic viscosity of a continuous wormlike cylinder with negligible end effects. It has been shown theoretically[37,38] for helical wormlike cylinders and straight cylinders that the neglect of the end effects is not allowed at very low values of L_r. Deviations from linearity observed with some plots of $(M^2/[\eta])^{1/3}$ vs. $M^{1/2}$ at low M are probably an indication of this effect. Anyway, evaluation of model parameters was not precluded by it.

Before concluding the discussion, we wish to recast the upper bounds to the use of eq 11 into a more practical form. It has been expressed in terms of L_r** (vide infra). Table III shows that the values of $L_{r,m}$ (the reduced contour length corresponding to the minimum point of the plot of $L_r^{1/2}/F_1$ vs. $L_r^{1/2}$) are generally much lower than L_r**. Thus, a decreasing trend of the plot of $M/[\eta]$ vs. $M^{1/2}$ (which is equivalent to the plot of $L_r^{1/2}/F_1$ vs. $L_r^{1/2}$) or a minimum on it may be an indication that the experimental data lie within the range of validity of eq 7 and 11. Since according to the argument given above the viscosity expansion factor α_η^3 is probably very close to unity at $L_r \lesssim L_{r,m}$, this criterion also holds for good solvent systems.

Acknowledgment. The author wishes to thank Professor H. Yamakawa for kindly making available the detailed numerical values of F_1. The assistance of Miss J. Vosyková in the computational work is gratefully acknowledged.

Registry No. Poly(*N*-hexyl isocyanate), 26746-07-6; schizophyllan, 9050-67-3; *catena*-μ-1,4-butadiynediyl-*trans*-bis(tributylphosphine)platinum, 64020-80-0; poly[ε-carbobenzoxy-L-lysine], 25931-47-9; poly[γ-ethyl L-glutamate], 25189-52-0; cellulose trinitrate, 9046-47-3; poly(*o*-phthaloyl-*trans*-2,5-dimethylpiperazine), 56467-11-9; poly(terephthaloyl-*trans*-2,5-dimethylpiperazine), 27576-10-9; poly(isophthaloyl-*trans*-2,5-dimethylpiperazine), 32031-91-7; (*S*)-poly[imino[1-oxo-2-[4-[[(phenylmethoxy)carbonyl]amino]butyl]-1,2-ethanediyl]], 25868-59-1; (*S*)-poly[imino[1-(3-ethoxy-3-oxopropyl)-2-oxo-1,2-ethanediyl]], 62978-01-2; phthalic acid/*trans*-2,5-dimethylpiperazine copolymer, 73310-67-5; terephthalic acid/*trans*-2,5-dimethylpiperazine copolymer, 27637-00-9; isophthalic acid/*trans*-2,5-dimethylpiperazine copolymer, 30324-14-2.

References and Notes

(1) Peterlin, A. *J. Chem. Phys.* **1960**, *33*, 1799.
(2) Peterlin, A. *J. Polym. Sci.* **1950**, *58* 473.
(3) Hearst, J. E. *J. Chem. Phys.* **1963**, *38*, 1062; **1965**, *42*, 4149.
(4) Eizner, Yu. E.; Ptitsyn, O. B. *Vysokomol. Soedin.* **1962**, *4*, 1725.
(5) Kurath, S. F.; Schmitt, C. A.; Bachhuber, J. J. *J. Polym. Sci., Part A* **1965**, *3*, 1825.
(6) Yamakawa, H.; Fujii, M. *Macromolecules* **1974**, *7*, 128.
(7) Tanner, D. W.; Berry, G. C. *J. Polym. Sci., Polym. Phys. Ed.* **1974**, *12*, 941.
(8) Tsvetkov, V. N.; Andreeva, L. N. *Adv. Polym. Sci.* **1981**, *39*, 95.
(9) Kovář, J.; Fortelný, I.; Bohdaneckỳ, M. *Makromol. Chem.* **1977**, *178*, 2375.
(10) Vitovskaya, M. G.; Tsvetkov, V. N. *Eur. Polym. J.* **1976**, *12*, 251.
(11) Morcelet, M.; Loucheux, C. *Biopolymers* **1978**, *17*, 593.
(12) Motowoka, M.; Norisuye, T.; Teramoto, A.; Fujita, H. *Polym. J.* **1979**, *11*, 665.
(13) Vošickỳ, V. *Acta Polym.* **1980**, *31*, 182.
(14) Tsuji, T.; Norisuye, T.; Fujita, H. *Polym. J.* **1975**, *7*, 558.
(15) Yamakawa, H. "Modern Theory of Polymer Solutions"; Harper and Row: New York, 1971.
(16) Bohdaneckỳ, M. Lecture at the 4th Microsymposium "Physik der Polymere", organized by the Technische Hochschule "Carl Schorlemmer", Leuna-Merseburg, Mar 1980. Preliminary results were presented, as a contribution to discussion, at the 25th International Symposium on Macromolecular Chemistry, Tashkent, Oct 1978.
(17) Motowoka, M.; Norisuye, T.; Fujita, H. *Polym. J.* **1977**, *9*, 613.
(18) Yamakawa, H.; Stockmayer, W. H. *J. Chem. Phys.* **1972**, *57*, 2843.
(19) Bohdaneckỳ, M.; Kovář, J.; Fortelný, I. 26th International Symposium on Macromolecular Chemistry, Mainz, 1979. Preprints of Short Communications, Vol. II, p 823.
(20) Berger, M. N.; Tidswell, B. M. *J. Polym. Sci., Part C* **1973**, *42*, 1063.
(21) Rubingh, D. N.; Yu, H. *Macromolecules* **1976**, *9*, 681.
(22) Berger, M. N.; Cervenka, A. *Eur. Polym. J.* **1974**, *10*, 205.
(23) Murakami, H.; Norisuye, T.; Fujita, H. *Macromolecules* **1980**, *13*, 345.
(24) Bur, A. I.; Fetters, L. J. *Chem. Rev.* **1976**, *76*, 727.
(25) Yanaki, T.; Norisuye, T.; Fujita, H. *Macromolecules* **1980**, *13*, 1462.
(26) Motowoka, M.; Norisuye, T.; Teramoto, A.; Fujita, H. *Polym. J.* **1979**, *11*, 665.
(27) Daune, M.; Freund, L.; Spach, G. *J. Chim. Phys.* **1962**, *59*, 485.
(28) Matsuoka, M.; Norisuye, T.; Teramoto, A.; Fujita, H. *Biopolymers* **1973**, *12*, 1515.
(29) Terbojevich, M.; Peggion, E.; Cosani, A.; D'Este, G.; Scoffone, E. *Eur. Polym. J.* **1967**, *3*, 681.
(30) Benoit, H.; Doty, P. *J. Phys. Chem.* **1953**, *57*, 958.
(31) Meyerhoff, G. *J. Polym. Sci.* **1958**, *29*, 399.
(32) Schulz, G. V.; Penzel, E. *Makromol. Chem.* **1968**, *112*, 260.

(33) Hunt, M. L.; Newman, S.; Scheraga, H. A.; Flory, P. J. *J. Phys. Chem.* **1956**, *60*, 1278.
(34) Huque, M. M.; Goring, D. A. I.; Mason, S. G. *Can. J. Chem.* **1958**, *36*, 952.
(35) Motowoka, M.; Fujita, H.; Norisuye, T. *Polym. J.* **1978**, *10*, 331.
(36) Sadanobu, J.; Norisuye, T.; Fujita, H. *Polym. J.* **1981**, *13*, 75.
(37) Yamakawa, H.; Yoshizaki, T. *Macromolecules* **1980**, *13*, 633.
(38) Yoshizaki, T.; Yamakawa, H. *J. Chem. Phys.* **1980**, *72*, 57.

Computer Simulation of the Dynamics of Star Molecules

R. J. Needs* and S. F. Edwards

Cavendish Laboratory, Cambridge CB3 0HE, United Kingdom. *Received December 16, 1982*

ABSTRACT: A computer simulation of 3-branched star molecules is presented in both free and highly entangled regimes. The diffusion constant of the center of mass of an entangled chain is shown to be of the form $D \propto N^{-b} \exp(-aN)$, where N is the number of chain segments in an arm, while the free-chain data are in good agreement with the Rouse result $D \propto N^{-1}$. A relaxation time of the entangled molecule is shown to be of the form $T \propto N^{d} \exp(cN)$ while the free-chain data agree with the Rouse result of $T \propto N^{2}$.

Introduction

In a series of papers by Evans and Edwards[1-3] a computer simulation of free and entangled linear molecules was presented. The presence of the other polymers in the melt was represented by a mesh of infinitely long rods. They found that the diffusion constant of the center of mass, D, and the relaxation time, T, defined as the time when the end-to-end vector correlation $\langle \mathbf{R}(t)\cdot\mathbf{R}(0)\rangle$ dropped to e^{-1} of its initial value obeyed

$$D \propto N^{-2.0(\pm 0.2)} \qquad T \propto N^{3.1(\pm 0.2)} \tag{1}$$

where N is the number of chain segments. This is in agreement with the reptation model of de Gennes.[4] In a later paper Evans[5] extended this work to 3-branched star molecules. For entangled stars he found

$$D \propto N^{-3.0(\pm 0.2)} \qquad T \propto N^{3.9(\pm 0.2)} \tag{2}$$

where N is the number of segments in an arm. de Gennes[6] has argued that, to diffuse, a 3-branched star molecule in a network of infinitely long, fixed obstacles would have to withdraw the end of one of its arms down its tube to the branching point and extend it, initially in the direction of another of the arms; see Figure 1. During the time scale of this process one could imagine the branching point as essentially fixed. He then calculated the probability of a configuration of an arm, with both ends coincident, in which the loop thus formed enclosed none of the obstacles, i.e., as in Figure 1b. He found that this probability P was given by

$$P(N) \propto \exp(-aN) \tag{3}$$

where a is a constant.[6,7] We have recalculated P, and for large N find

$$P(N) \cong \frac{2(2^{1/2})z}{\pi^{1/2}N^{1.5}(z-1)} \exp(N \log (2(z-1)^{1/2}) - N \log (z)) \tag{4}$$

where z is the coordination number of the lattice.[14] As one of these retracing configurations must be intermediate to a diffusion or relaxation step, he argued that the diffusion constant would be proportional to this probability and the relaxation or renewal time to its inverse. Clearly this cannot be exact; different configurations should have different weights, but we have no way to calculate the weights and so assume them all equal.

It is important to note that the de Gennes mechanism is not the only possible one. If the branching point were to move p steps down the tube of one arm, dragging the other two arms behind it, one of these two arms which occupy p steps of the same tube would only have to disengage the remaining $N - p$ steps for a diffusive step to occur. We can sum all the configurations intermediate to one of these diffusive steps to give a total probability $M(N)$.

$$M(N) = \sum_{p=0}^{N/2} P(2N - 2p)\{1 - P(2p)\} \tag{5}$$

where we define $P(0) = 0$. The $p = N/2$ term is the de Gennes mechanism.

Doi and Kuzuu[8] have used arguments based on the dynamics of an arm to calculate the same form for T. They then predict the forms of the creep compliance and viscosity of a melt of such stars, which are in good agreement with the data of Graessley and Roovers.[9]

Model

The computer model is exactly that of Evans.[5] Only a brief description of the model is given here as a full description has already been published.[1,5] The polymer is modeled as a set of M points on a cubic lattice; the separation of neighboring points on the chain is one lattice spacing. No excluded volume interaction is used between points along the polymer. This ensures that the chain will have ideal chain statistics as is well-known to be the case in melts. A chain, linear or branched, is set up as a random walk on the lattice. Points along the chain are chosen at random and moved such that the chain remains connected and no portion of the chain has moved through any obstacles present. A time step is M such attempted moves. The obstacles are infinitely long rods located on a cubic lattice shifted from the polymer lattice in each of the Cartesian directions by $^1/_2$ a lattice spacing. This set of obstacles is called the "cage". In this simulation obstacles were placed at each possible site; thus the distance between obstacles was the polymer step length. Previous simulations[1-3,5] used variable cage spacings, but as the molecule is most highly entangled with a cage spacing of 1, this spacing was used throughout.

As the model neglects both hydrodynamic and excluded volume interactions, it is not successful at modeling polymers in dilute solution. But if no obstacles are present and we model a free chain, we retrieve the results of the Rouse chain.[11] In particular, Evans found for both linear

0024-9297/83/2216-1492$01.50/0